EXPERIMENTAL AND NUMERICAL INVESTIGATION OF FLOW MALDISTRIBUTION IN A CIRCULAR MICROCHANNEL HEAT EXCHANGER AT VARIOUS FLOWRATES

ALAA D.J. AL-BAYATI[1], HASANAIN A. ABDULWAHHAB[2],
HUSSAIN. H. AL-KAYIEM[3, *], IBRAHIM. M. MOHAMED[4]

[1]Chemical Engineering Department, Al-Mustaqbal University College, Hilla, Iraq
[2]Training and Workshop Centre, University of Technology-Iraq, Baghdad, Iraq
[3]Hilla University College, Babylon, Iraq
[4]Mechanical Engineering Department, Universiti Teknologi PETRONAS,
32610 Seri Iskandar, Perak, Malaysia
*Corresponding Author: prof.hussain@acaress.org

Abstract

Configuration of the microchannels connection to the manifold in microchannel heat exchangers significantly influences flow uniformity in the microchannels and significantly affects the even thermal dissipation to the surroundings. This paper presents the uniformity anxieties of the flow through a non-protruded microchannel heat exchanger that has been explored experimentally and numerically. The prototype consisted of 5-mm-diameter inlet and outlet headers with 20 microchannels of 0.96-mm-diameter and 50-mm-long with no protrusion depth. The velocities were measured by particle image velocimetry at 308 and 617 ml/min flow rates, corresponding to Reynolds numbers of 1500 and 3000 based on the header diameter. Using ANSYS FLUENT, a CFD simulated the flow in the microchannels heat exchanger at Reynolds numbers of 1500, 3000, 4500, 6000, and 7500, allowing a detailed flow field visualization. The numerical procedure was validated by comparing the simulation velocity results with the experimental results, showing a mean relative error of all the 20 microchannels of 3.8% and 8.2% for flow rates of 308 and 923 ml/min, respectively. Both experimental and numerical results show that the microchannels' velocity distribution is not uniform at the last few microchannels. The present work results support the concept of a protruded microchannel that produces better uniform flow. Hence, extended investigations are recommended to explore the effect of the channel's protrusion on flow uniformity and address the high inconsistency in the pressure drop prediction. Also, the simulation could be beneficial if extended to compare the maldistribution with various manifold diameters.

Keywords: Flow maldistribution, Flow uniformity, Manifolds, Microchannel
        heat exchanger.

1.Introduction

Microdevices' dominant features are the high ratio of surface area to volume, the effective internal volume of microdevices is very small, and the flow is mostly laminar. In their review article, Lerou et al. [1] discussed some of the advantages of a microchannel heat exchanger (MCHE). The fluid flow is vastly distributed, requiring only a shorter flow length through microchannels. So, the overall pressure drop is lower than in the conventional heat exchanger. In industries, the micro-channel heat exchanger provides a smaller footprint, lower capital and operating expenditure, and higher system capacity for the same compression capacity. Even with the advantages stated above, the industry still faces several challenges in designing a performance-wise optimized MCHE. One major problem is the refrigerant's maldistribution flowing from the header into the microchannels.

A simplified 2-D view of the micro-channel heat exchanger with a single pass is shown in Fig. 1. The fluid entering the manifold is distributed to the various tubes. There will be a maldistribution of flow as equal flows entering the whole channels are not achieved.
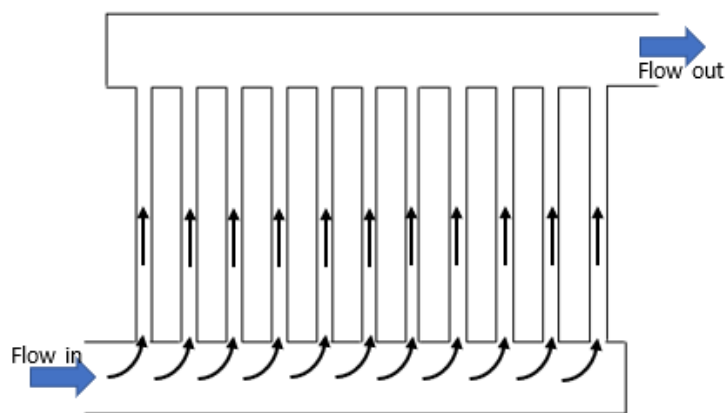
Fig. 1. 2D Configuration of a microchannel heat exchanger.

It has been experimentally shown by Liu and Garimella [2] that fully turbulent flow is less likely to happen in a microchannel (MC) (with a hydraulic diameter of less than 1 mm). Wen et al. [3] used CFD simulation in FLUENT and Particle Image Velocimetry (PIV) to determine the turbulent flow structure inside the entrance of a plate-fin heat exchanger. The simulation and the experiment were conducted under the same inlet Reynolds number of $Re = 6.0 \times 104$. The authors conclude that PIV and CFD are well-suited for analysing intricate flow patterns. Their numerical findings indicate that fluid maldistribution efficiency at the traditional entrance has declined. With a punched baffle, the enhanced design can effectively increase performance in both radial and axial directions.

Foli et al. [4] introduced multi-objective genetic algorithms to determine MCs' optimal geometric parameters in the MCHE to achieve a maximum heat transfer rate under the required design constraints. CFD analysis was also performed with an analytical method of calculating the optimal geometric parameters. They advised that the experimental research has shortcomings, such as many data errors and

failure to cover all heat exchanger conditions. Therefore, the numerical simulation of nonuniform flow is a crucial issue.

Alnaimat and Mathew [5] investigated the fluid distribution in multichannel microfluidic devices with U-shaped manifolds at various flowrates and channel width and spacing. The model has 50 microchannels with water as the working fluid. The flow distribution in the microfluidic device is investigated for microchannel widths between 100 µm to 500 µm and Reynolds numbers ranging between 0.04 to 100. Results show that an increase in Reynolds number increases the nonuniformity of the flow. Pressure and flow distribution have been investigated and presented in contour plots.

A numerical analysis of the flow patterns of compact plate-fin heat exchangers was conducted by Sheik et al. [6] since air (gas) flow maldistribution in the headers impacts the exchanger's efficiency. Three standard compact plate-fin heat exchangers were analysed using Fluent software to measure flow maldistribution's effects with ideal and actual cases in their analysis.

The effect of maldistribution is illustrated quantitatively by Chin and Raghavan [7]. They reported that maldistributed flow could account for a net reduction of 2.2% in thermal performance and a net increase of 62.8% in mass-averaged pressure drop. Maldistribution is never advantageous and is always adverse in a heat exchanger. The aforementioned adverse effect can only be minimized by decreasing the standard deviation of the flow distribution. The event of flow maldistribution in the header is hardly preventable in the presence of several head losses, geometrical configurations, or unknown factors. The mass flow rate of refrigerant entering each micro-channel is not always uniform throughout the manifold.

The effects of nonuniform flow on the heat exchanger performance have been well investigated over the decades. Jiao et al. [8] have shown that the flow distribution efficiency in the heat exchanger is effectively improved by the optimum design of the second header installation through experimental studies. The findings show that when the outlet pipe diameter to the inlet pipe diameter ratio of the two headers of the heat exchanger is equal, the flow distribution becomes more uniform.

Bobbili et al. [9] performed experimental investigations to find the pressure drop and flow through the port to the channel in the plate heat exchangers for a wide variety of Reynolds numbers. The results showed that the flow maldistribution increases with an increase in the total pressure drop in the heat exchangers.

The maldistribution problem has been studied numerically by many researchers (e.g., Lu et al. [10], Pan et al. [11], Tonomura et al. [12], Tong et al. [13], Kim et al. [14], Lee et al. [15]). Countless contributions made by various researchers are yet to be listed here. Until recently, several related models and solution methods have been thoroughly integrated by Liu and Garimella [2] into one theoretical framework. The results discussed in Ke et al. [16] investigation focus on a problem similar to Fig. 1, i.e., where no protrusion effect was considered. Dąbrowski et al. [17] conducted experimental investigations on the channel blockage and flow maldistribution during unsteady flow in a model microchannel plate heat exchanger. They concluded that channel blocking could only occur between the end of the channels and the outlet collector. The increase in the flow resistance and the pressure drop for the increasing flow rates is also a reason for the blockage. A review paper by Xiong et al. [18] presented the research progress on the

hydrothermal and drainage performance of MCHEs. They focused on the type of MCHE under frosting, defrosting, and wet conditions. They summarised the experimental research on the frosting and drainage characteristics of MCHEs and introduced three methods for improving the frosting and defrosting performance.

However, there is a clear shortage in the literature on two issues related to the MCHE. First is the lack of flow structure analysis in MCHE with circular tubes. Second, no sufficient analysis and information on the header diameter effect on the maldistribution and the flow uniformity. Wen et al. [3] and Borreani et al. [19] recommended combining CFD and experimental tests to analyse microchannel flows, and this study adopted their recommendation.

Based on the identified research gap, this paper presents insight into the flow within the MCHE to address the flow nonuniformity issue. The selected MCHE is a tubular type with a circular cross-section that comprises inlet and outlet headers of 5 mm diameter and 20 microchannels of 1 mm diameter. As such assessment requires flow visualization, the analysis is mostly obtained by validated CFD simulation, while the experimental findings are used to validate the numerical procedure. The flow in each channel is measured by particle image velocimetry (PIV) at various Reynolds numbers ranging from 1500 to 7500. The CFD is achieved by simulation in ANSYS FLUENT software. The CFD simulated the MCHE at Reynolds numbers of 1500, 3000, 4500, 6000, and 7500 to explore the flow rate contribution on the uniformity and maldistribution in the MCs. The investigation has not considered any thermal analysis, as the project focuses on the nonuniformity of the MCs' flow.

2. Methodology

Wen et al., 2006 used the PIV and CFD to investigate the flow pattern in a flat plate heat exchanger, and they recommended the use of CFD and PIV to investigate flow issues in MCHEs. Their recommendation is adopted in the current investigation. An experimental setup has been designed and fabricated, and a computational model has been developed for CFD simulation. The experimental measurements, using PIV, provided benchmark data for validation of the CFD simulation.

However, to calculate the overall maldistribution coefficient, ϕ in each of the three different header diameters with various flow rates, Eq. (1) recommended by Dąbrowski et al. [17] has been adopted, with N = 20 channels.

$$\Phi_i\% \ = \ \frac{\sum_{i=1}^{N}\Phi_i}{\sqrt{N}} \times 100 = \frac{1}{\sqrt{N}}\sum_{i=1}^{N}\frac{|V_i-V_m|}{V_m} \times 100 \tag{1}$$

2.1. Experimental setup

The model has three main parts: inlet header, outlet header, and microchannels. The entire flow passages, including the inlet header, outlet header, and microchannels, considered throughout this work, are constant in their cross-sectional area.

The geometrical parameters in the current investigation to design and fabricate the MCs are adopted from the industrial MCs used by Khan and Fartaj [20]. The values of the geometries are shown in Table 1.

Figure 2 shows the assembled MCHE. The MCHE was fabricated using the SLA 3D printing method with a clear resin, allowing the instrumentation to capture

the prototype's flow. The prototype was made of male and female parts facing each other and tightened by bolts and screws.

Table 1. Constant parameters of the microchannel heat exchanger.

Constant Parameters	Value
Channel type	Circular channel
Header diameter (Manifold Diameter), Dh	5 mm
Outflow port diameter, Dc	0.96 mm
Channel Spacing, S	0.96 mm
Length of the manifold, L	60 mm
Number of ports, n	20
Length of port (Microchannel length)	50 mm
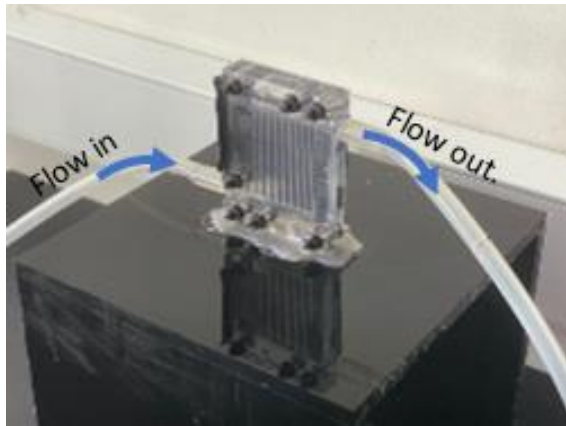
Fig. 2. 3D printed microchannel heat exchanger.

The experimental setup is shown schematically in Fig. 3. Water flow is discharged and controlled by a Peristaltic pump through a 6.4-mm-diameter plastic tube connected to the 5-mm-diameter inlet header of the MCHE. Water flows up in 20 MC risers with 0.96-mm-diameters and exits at the top into the 5-mm-diameter outlet header. A digital differential pressure manometer is connected at the headers inlet and out to measure the pressure drop across the MCHE.
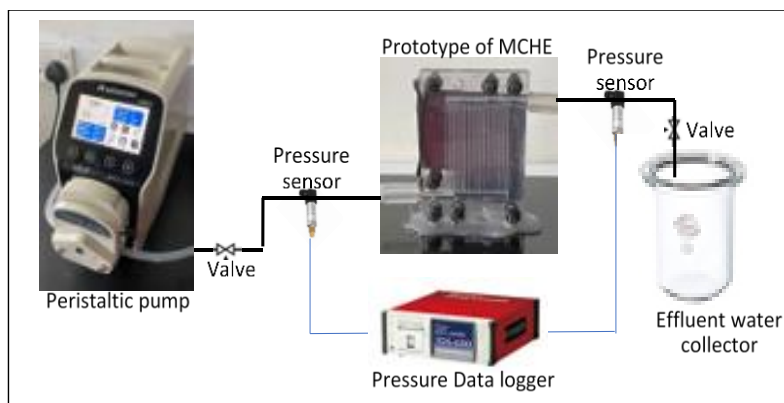
Fig. 3. Schematic of the experimental setup.

2.2. Numerical method

In their experimental and numerical investigations, Liu and Garimella [2] have demonstrated that the flow analysis of MCHE by commercial software packages is satisfactory and can aid the study of flow characteristics in MCs. Accordingly, to reduce the time and cost of a wide range of Re, ANSYS Fluent 2020 R1 commercial software has been used in the current investigations to extend the investigation from two Reynolds numbers in the experiment to five Reynolds numbers in the simulation. The model was simulated with five different flow rates of 308, 617, 923, 1234, and 1543 ml/min, covering corresponding Reynolds numbers of 1500, 3000, 4500, 6000, and 7500.

2.2.1. Computational model and boundary conditions

The computational fluid dynamic (CFD) software ANSYS Fluent 2020 R1 was used to solve the three-dimensional fluid flow equations. The simulation was performed with the help of a pressure-based solver. The fluid flow in the MCHE was assumed to be steady-state and incompressible. The fluid is water at room temperature of 25 ºC with a density of 998.2 kg/m3 and viscosity of 0.001 kg/s. The fluid flows from the down inlet header, enters the MCs from the bottom, passes through the micro-channels, proceeds upward, and exits from the outlet header, as shown in Fig. 4.
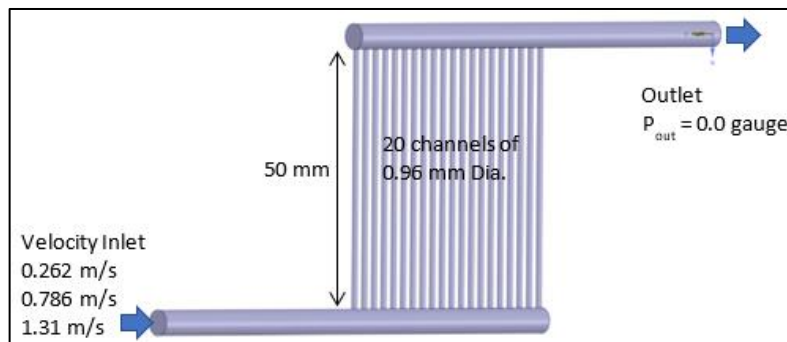
Fig. 4. Computational model of the MCHE in ANSYS-FLUENT.

This paper focuses on the flow distribution inside the micro-channel heat exchanger, not the walls' heat transfer. The geometry was extracted using a volume extractor using space claim on ANSYS Fluent 2020 R1 with the same volume dimensions as the real prototype used at the experiment, and wall thickness was neglected. The gravity effect on the flow is negligible.

2.2.2. Meshing criteria

The meshing process was challenging as the MCHE's geometry in total was tiny, mostly since the micro-channel was in micro size. The best accurate results were achieved with the smallest mesh possible. The meshing was done in two phases: meshing the inlet and outlet headers and micro-channel ports. Both meshing phases were done separately with different mesh sizes. The mesh used in the setup has a total of element number 11.432 million with an excellent average aspect ratio of $1.85 < 5$ and an average orthogonal quality of 0.772.

2.2.3. Mesh independency check

A grid independence test was performed to obtain the most convenient mesh structure, ensuring high accuracy with less computational time. The number of mesh elements was changed from 4.909 million to 11.432 million for the Re of 1500 in the test. Table 2 briefly demonstrates the relative error defined in Equation (2) between the grid (G1) and the other grids (G2, G3, and G4). It has been concluded that the computational model with 11.432 million provided a reasonable error for the average velocity value at a fixed point inside the MCHE compared to the other models with a different number of elements.

$$e\% = \left| \frac{V_i - V_{i-1}}{V_i} \right| \times 100 \tag{2}$$

Table 2. Mesh independency test.

No.	Re	Grid Number	Velocity (m/s)	Error %
1	1500	4,909,915	0.2435	-
2	1500	6,325,274	0.2450	0.61
3	1500	8,378,822	0.2449	0.57
4	1500	11,432,581	0.2447	0.49

2.2.4. Governing equation

The governing equations of incompressible flow in the MCHE are provided by Munson et al. [21], Hasan and Tbena [22], and Bayrak et al. [23]: Continuity and momentum equations for steady-state, incompressible, and 3D fluid flow have been used. They can be expressed respectively:

Flow transforms from laminar characteristics to turbulent characteristics. The realizable k-ε model with scalable wall function and default settings of the model constants was chosen to solve the continuous flow [24]. The realizable k-ε is based on modified transport equations for an alternative formulation for the turbulent kinetic energy, k, and its dissipation rate, ε.

The transport equations for k and ε, in the realizable k- ε model Arie et al. [25], are represented below in Eqs. (3) and (4), respectively.

$$\frac{\partial y}{\partial x_j}(\rho k u_j) = \frac{\partial}{\partial x_j}\left[(\mu + \frac{\mu_t}{\sigma_k})\frac{\partial k}{\partial x_j}\right] + G_k + G_b + \rho_\varepsilon + Y_M + S_k \tag{3}$$

$$\frac{\partial}{\partial x_j}(\rho \varepsilon u_j) = \frac{\partial}{\partial x_j}\left[(\mu + \frac{\mu_t}{\sigma_\varepsilon})\frac{\partial \varepsilon}{\partial x_j}\right] + \rho C_1 S_\varepsilon + \rho C_2 \frac{\varepsilon^2}{k+\sqrt{v_\varepsilon}} + C_{1\varepsilon}\frac{\varepsilon}{k}C_{3\varepsilon}G_b + S_\varepsilon \tag{4}$$

where, $C_1 = max\left[0.43 \frac{\eta}{\eta+5}\right]; \eta = S\frac{k}{\varepsilon}; S = \sqrt{2S_{ij}S_{ij}}$

In these equations, G_k characterizes the production of turbulence kinetic energy due to the mean velocity gradients, G_b is the initiation of turbulence kinetic energy due to the buoyancy effect, Y_M represents the involvement of the fluctuating turbulence in the overall dissipation rate, C_2 and $C_{1\varepsilon}$ are constants. σ_k and σ_ε are the turbulent Prandtl numbers for k and ε, respectively. S_k and S_ε are user-defined source terms. The model constants have been determined to guarantee that the model operates well for specific undisputed flows Hanjalic and Launder [26]. The function of Prandtl numbers σ_k and σ_ε is to connect the diffusivities of k and ε to the eddy viscosity μ_t. So that its effect is accounted for within the gradient diffusion

term of the turbulent transport equations Versteeg and Malalasekera [27]. η is the expansion parameter, which is defined as the ratio of the turbulence to the mean-strain time scales. And S_{ij} is the strain-rate tensor, which is calculated indirectly by using the gradient transport hypothesis presented in Tsan-Hsing et al. [28]. Therefore, the following constants have been established by a comprehensive data fitting for the realizable *k-ε* model Versteeg and Malalasekera [27].

$$C_{1\varepsilon} = 1.44, \qquad C_2 = 1.92, \qquad \sigma_k = 1.0, \qquad \sigma_\varepsilon = 1.2$$

3. Results and Discussion

The experimental velocity measurements were carried out at Re values of 1500 and 3000 with 5-mm-diameter headers. The pressure measurements were carried out at 1500, 3000, 4500, 6000, and 7500. The numerical simulations were carried out at 1500, 3000, 4500, 6000, and 7500, where detailed pressure, velocity, and flow patterns were obtained. The experimental measurements at 1500 and 3000 Re were used to validate the numerical procedure. The simulation inputs are constant, except the inlet velocity and pressure are changeable. The input boundary conditions for each flow rate are shown in Table 3.

Table 3. Input variable used at the 5-mm-diameter inlet header as boundary conditions to ANSYS-FLUENT.

Flow rate (ml/min)	Reynolds Number	Velocity (m/s)	Pressure (kPa)
308	1500	0.262	2.2
617	3000	0.524	6.2
923	4500	0.786	11.5
1234	6000	1.048	20
1543	7500	1.310	30.5

3.1. Validation of numerical procedure

The present simulation was validated by comparing the numerical results with experimental measurements. The experiment was conducted for 308 and 617 ml/min flow rates, corresponding to Re of 1500 and 3000, respectively.

The experimental data validated the numerical results, as shown in Table 3. The numerical and experimental results show the fluid's velocity inside MCs 1, 10, and 20 at Re 1500 and 3000 flow rates. The maximum relative error percentage between the numerical and experimental results is 6.8% and 9.16 % for Re of 1500 and 3000, respectively. The mean relative percentage of error of all compared cases is 5.6%, indicating a good agreement and proving validation of the computational simulation procedure.

Table 4. CFD simulation prediction and experimental measurement of velocity results with the relative error percentage.

Micro-channel	Velocity at Re 1500 (m/s)		Relative error (%)	Velocity at Re 3000 (m/s)		Relative error (%)
	Sim.	Exp.		Sim.	Exp.	
MC - 1	0.337	0.323	4.04	0.633	0.593	6.05
MC - 10	0.330	0.316	4.38	0.633	0.575	9.16
MC - 20	0.381	0.355	6.85	0.733	0.711	2.93

3.2. Qualitative analysis

The experimental results have been accomplished using PIV. The results of the flow structure were mapped as velocity vectors in each channel. Figure 5 shows the particle image velocimetry measurements' scalar map, where this map represents the velocities inside the MCs of the MCHE.
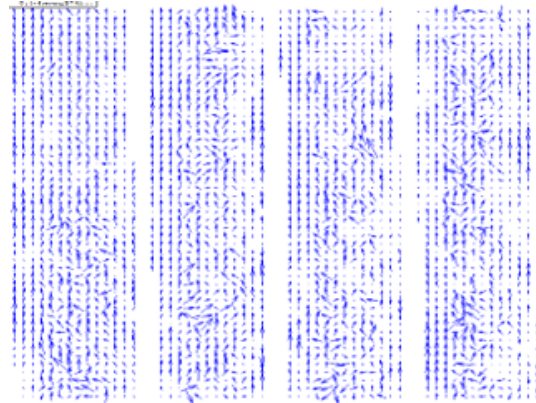
**Fig. 5. Scalar mapping of the particle
image velocimetry measurement results.**

Figure 6 shows the velocity contours at Re of 1500. The fluid's inlet angle was large when fluid flowed into the channel, which caused a clear flow separation and a strong eddy current at the channel's inlet. The flow is slowing down as moving downstream in the inlet header. The velocity flow field differs from one MC to another. The flow velocity in the last MC is higher than in the first MC. The right-side velocity vector figures are enlarged sections for better clarification.
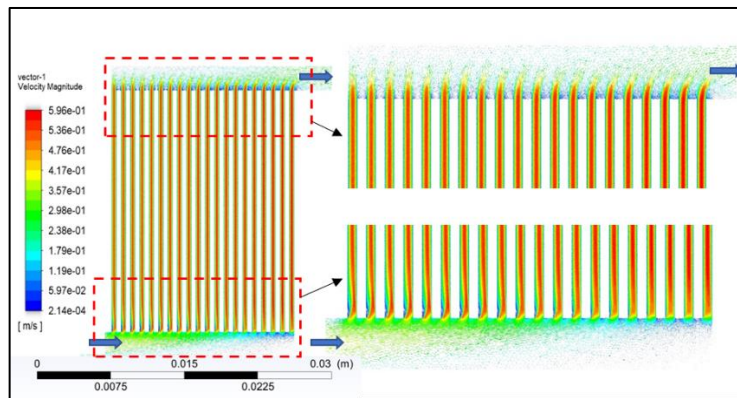
**Fig. 6. The velocity vector field in the MCHE at Re = 1500
with enlarged segments at the microchannels' inlets and outlets.**

Circulation and dead zones exist in some flow regions. A nearly zero velocity zone is present at the inlet header's end. The reason is that most of the fluid is already flowing inside the MCs, and velocity is decreasing towards the close end

of the header. In the lower end corner, there is a completely dead zone with almost standstill water particles. This is also can be visualized in the velocity vector shown in Fig. 6. However, there is still water flowing up in the last MC.

The flow field in the MCHE in terms of the velocity vector at Re = 7500 is presented in Fig. 7. The figure shows the entire MCHE and enlarged segments of the inlets and outlets of the MCs. The trend of flow behaviour is similar to the case of flow with Re = 1500. However, the distortion and nonuniformity are more obvious due to the higher velocity in each MC. For the flow to reach the fully developed status, it requires a shorter distance than in the case of Re = 1500.
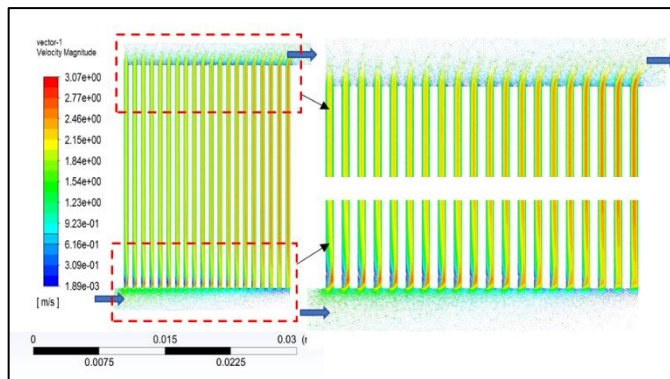
**Fig. 7. The velocity vector field in the MCHE at Re = 7500
with enlarged segments at the inlets and outlets of the microchannels.**

3.3. Quantitative analysis

The simulation's predicted mean velocity is presented in Fig. 8 in a comparative histogram for MCs 1, 10, and 20 at various Re of 1500, 3000, 4500, 6000, and 7500. The flow is nonuniform as the difference percentage of the velocity between channels 1, 10, and 20 is more than 10% at Re 1500, 3000, and 4500 flow rates. Furthermore, the nonuniformity increases with a higher flow rate, at Re 6000 and 7500, where the velocities difference between becomes more than 15%. The flow velocity in channel 20 is considerably higher at all flow rates than MCs 1 and 10, which proves the misdistribution concept.
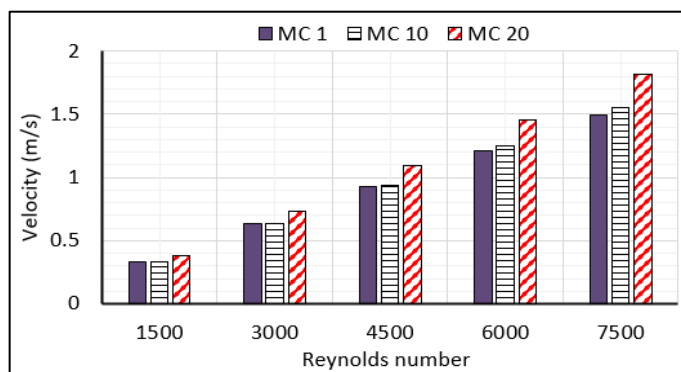
Fig. 8. Predicted velocity inside the microchannels 1, 10 and 20.

4. Conclusions

Flow nonuniformity in non-protruded microchannel heat exchangers is investigated in the current research experimentally and computationally. ANSYS Fluent 2020 R1 was used to simulate the flow distribution inside the heat exchanger's microchannels at the five different flow rates referring to Reynolds numbers 1500, 3000, 4500, 6000, and 7500. The numerical procedure is validated by comparing the experimental results with a mean relative error percentage of 5.56%. The results indicated the existence of flow maldistribution and nonuniformity in the examined microchannel heat exchanger, as the flow distribution differs in the 20 microchannels in all cases of flow rates. The velocities in the latest microchannels are higher than in the early microchannels. The increment of the velocity values in the microchannels is not uniform or consistent. All tested flow cases showed that the flow increases gradually in microchannels 1 to 9 and suddenly reduces in microchannel 10. Then, the flow increases gradually in microchannel 11 up to 20.

An important finding, which requires further independent study, is the structure of the flow exit from the microchannels into the outlet header in the shape of jet flow. This observation justifies the discrepancy in predicting the pressure drop in microchannels. Extending the study with a focus on the pressure drop in the microchannels is highly recommended. Also, it is recommended to explore the effect of the header diameters on the flow maldistribution in the circular microchannel heat exchanger.

References

1. Lerou, J.J.; Tonkovich, A.L.; Silva, L.; Perry, S.; and McDaniel, J. (2010). Microchannel reactor architecture enables greener processes. *Chemical Engineering Science*, 65, 380-385.

2. Liu, D.; and Garimella, S.V. (2004). Investigation of liquid flow in microchannels. *Journal of Thermophysics and Heat Transfer,* 18, 65-72.

3. Wen, J.; Li, Y.; Zhou, A.; and Zhang, K. (2006). An Experimental and numerical investigation of flow patterns in the entrance of plate-fin heat exchanger. *International Journal of Heat and Mass Transfer*, 49, 1667-1678.

4. Foli, K.; Okabe, T.; Olhofer, M.; Jin, Y.; and Sendhoff, B. (2006). Optimization of micro heat exchanger: cfd, analytical approach and multi-objective evolutionary algorithms. *International Journal of Heat and Mass Transfer*, 49, 1090-1099.

5. Alnaimat, F.; and Mathew, B. (2023). Flow distribution in microchannel devices with u-shaped manifolds. *International Journal of Thermofluids*, 19, 100391.

6. Ismail, L.S.; Ranganayakulu, C.; and Shah, R.K. (2009). Numerical study of flow patterns of compact plate-fin heat exchangers and generation of design data for offset and wavy fins. *International Journal of Heat and Mass Transfer*, 52(17-18), 3972-3983.

7. Chin, W.M.; and Raghavan, V.R. (2011). On the adverse influence of higher statistical moments of flow maldistribution on the performance of a heat exchanger. *International Journal of Thermal Sciences*, 50, 581-591.

8.   Jiao, A.; Zhang, R.; and Jeong, S. (2003). Experimental investigation of header configuration on flow maldistribution in plate-fin heat exchanger. *Applied Thermal Engineering*, 23, 1235-1246.

9.   Bobbili, P.R.; Sunden, B.; and Das, S.K. (2006). An Experimental investigation of the port flow maldistribution in small and large plate package heat exchangers. *Applied Thermal Engineering*, 26, 1919-1926.

10. Lu, F.; Luo, Y.H.; and Yang, S.M. (2008). Analytical and experimental investigation of flow distribution in manifolds for heat exchangers. *Journal of Hydrodynamics, Series B,* 20, 179-185.

11. Pan, M.; Tang, Y.; Pan, L.; and Lu, L. (2008). Optimal design of complex manifold geometries for uniform flow distribution between microchannels. *Chemical Engineering* Journal, 137, 339-346.

12. Tonomura, O.; Tanaka, S.; Noda, M.; Kano, M.; Hasebe, S.; and Hashimoto, I. (2004). CFD-Based optimal design of manifold in plate-fin microdevices. *Chemical Engineering Journal*, 101, 397-402.

13. Tong, J.C.K.; Sparrow, E.M. and Abraham, J.P. (2009). Geometric strategies for attainment of identical outflows through all of the exit ports of a distribution manifold in a manifold system. *Applied Thermal Engineering*, 29, 3552-3560.

14. Kim, D.; Yu, C.H.; Yoon, S.H.; and Choi, J.S. (2011). Effects of manifold geometries on flow distribution to parallel microchannels. *Journal of Mechanical Science and Technology,* 25, 3069-3074.

15. Lee, A.K.; Park, N.S.; Kim, S.; and Kim, N. (2012). Physical modifications to improve a channel's flow distribution. *Korean Journal of Chemical Engineering*, 29, 201-208.

16. Ke, H. et al. Lin, Y.; Ke, Z.; Xiao, Q.; Wei, Z.; Chen, K.; and Xu, H. (2020). Analysis exploring the uniformity of flow distribution in multichannels for the application of printed circuit heat exchangers. *Symmetry*, 12(2), 314.

17. Dąbrowski, P.; Klugmann, M.; and Mikielewicz, D. (2019). Channel blockage and flow maldistribution during unsteady flow in a model microchannel plate heat exchanger. *Journal of Applied Fluid Mechanics*, 12(4), 1023-1035.

18. Xiong, T.; Liu, G.; Gao, Q., Yan, G.; and Yu, J. (2023). Thermal-Hydraulic and drainage performance of microchannel heat exchangers for refrigeration and heat pump systems under frosting, defrosting, and wet conditions: a comprehensive review. *Journal of Building Engineering*, 64(1), 105654.

19. Borreani, W.; Devia, F.; Lomonaco, G.; and Marchitto, A. (2017). CFD initial assessment of a protrusions based experimental facility. *International Journal of Heat and Technology*, 35(S1), S270-S280.

20. Khan, M.G.; and Fartaj, A. (2011). A Review on microchannel heat exchangers and potential applications. *International Journal of Energy Res*earch, 35, 553-582.

21. Munson, B.R.; Okiishi, T.H.; Huebsch, W.W.; and Rothmayer, A.P. (2013). *Fundamentals of Fluid Mechanics,* Seventh Edition, Wiley.

22. Hasan, M.I.; and Tbena, H.L. (2018). Numerical investigation of microchannel heat sink with MEPCM suspension with different types of PCM. *Al-Qadisiyah Journal for Engineering Sci*ences, 11(1), 115-133.

23. Bayrak, E.; Olcay, A.B.; and Serincan, M.F. (2019). Numerical investigation of the effects of geometric structure of microchannel heat sink on flow characteristics and heat transfer performance. *International Journal of Thermal Sciences*, 135, 589-600.

24. ANSYS Fluent User' s Guide, 2013.

25. Arie, M.A.; Shooshtari, A.H.; Dessiatoun, S.V.; Al-Hajri, E.; and Ohadi, M.M. (2015). Numerical modeling and thermal optimization of a single-phase flow manifold-microchannel plate heat exchanger. *International Journal of Heat and Mass Transfer*, 81, 478-489.

26. Hanjalic, K.; and Launder, B. (2012). *Modelling Turbulence in Engineering and the Environment*. Cambridge University Press, UK.

27. Versteeg, H.K.; and Malalasekera, W. (2007). *An Introduction to computational fluid dynamics: the finite volume method*. Pearson education.

28. Tsan-Hsing, S.; William, W.L.; Aamir, S.; Zhigang, Y.; and Jiang, Z. (1995). A New k-$\acute{\varepsilon}$ eddy viscosity model for high Reynolds number turbulent flows. *Computers & Fluids*, 24(3), 227-238.